RSC Advances

PAPER

View Article Online
View Journal | View Issue



Cite this: *RSC Adv.*, 2022, **12**, 26362

# Hydrothermal synthesis of multi-cationic high-entropy layered double hydroxides†

Amy J. Knorpp, ‡*[a] Anna Zawisza,‡[ab] Shangxiong Huangfu,[a] Aurelio Borzì,[c] Adam H. Clark, [d] Dariusz Kata,[b] Thomas Graule[a] and Michael Stuer *[a]

Received 30th August 2022
Accepted 31st August 2022

DOI: 10.1039/d2ra05435c

rsc.li/rsc-advances

High-entropy materials are compositionally complex materials which often contain five or more elements. The most commonly studied materials in this field are alloys and oxides, where their composition allows for tunable materials properties. High-entropy layered double hydroxides have been recently touted as the next focus for the field of high-entropy materials to expand into. However, most previous work on multi-cationic layered double hydroxides has focused on syntheses with 5 or less cations in the structure. To bridge this gap into high-entropy materials, this work explores the range and extent of different compositional combinations for high-entropy double layered hydroxides. Specifically, pure layered double hydroxides were synthesized with different combinations of 7 cations (Mg, Co, Cu, Zn, Ni, Al, Fe, Cr) as well as one combination of 8 cations by utilizing a hydrothermal synthesis method. Furthermore, magnetic properties of the 8-cation LDH were investigated.



## 1. Introduction

In the last two decades, the concept of high-entropy materials has become a subject that has garnered increasing attention in the material science community. What has drawn particular interest is their tunable material properties across many different applications. Initially, alloys based on combinations of five or more elements in near-equimolar compositions were designed.[1,2] The main idea behind these materials is to maximize configurational entropy in order to minimize the Gibbs free energy ($\Delta G = \Delta H - T\Delta S$), thus stabilizing a system towards robustness and tunability. Furthermore, the large number of elements incorporated in the structure may lead to cocktail effects resulting in unexpected materials properties that would not be otherwise exhibited by each element individually.[3]

The field of research on HEMs (HEMs – High Entropy Materials) has expanded significantly and today includes not merely HEAs (HEAs – High Entropy Alloys), but also oxides,[4] diborides,[5] carbides,[6] nitrides,[7] polymers,[8] fluorides[9] or sulfides.[10] With the expanding portfolio of HEMs, there is conjecture in the HEM community[11,12] of other potential materials that could benefit from high-entropy configurations. One such material class are hydroxides, specifically layered double hydroxides (LDH).[13,14] These materials have also been referred to by several other names or abbreviations, including high-entropy hydroxides (HEH), high-entropy layered hydroxides (HELH), or high-entropy layered double hydroxides (HE-LDH).

Layered double hydroxides (LDHs), also known as hydrotalcite-like compounds (when obtained synthetically), are a large family of anionic clay materials, which can be represented by the formula $[M^2_{1-x} + M^3_x + (OH)_2]A^n_{x/n} \cdot mH_2O$, where M is a metal and A is a $n$-valent anion. The structure of LDHs includes brucite-like sheets separated by anionic species and water.[14,15] LDHs with various cations substituted into the structure are widely used in many fields, such as catalysis,[16,17] biomedical science,[18,19] environmental remediation,[20,21] polymerization,[15] and electrochemistry.[22] Additionally, LDHs can be used as precursors for such oxides structures like spinel[23] where the incorporation of a few cations in the LDH can be used to tailor the spinel's final chemistry and shape/size.[24–26]

The expansion of high-entropy materials to LDHs is a logical one, as different transition metal cations can readily be substituted into their crystal structure.[13,14] However, high-entropy layered double hydroxides remains largely unexplored since most attention has been on incorporating two or three cations rather than the number of incorporated cations relevant to high-entropy materials.

Recently a universal configurational entropy metric (labelled EM) has been proposed that accounts for complex crystal structures as well as multiple sub lattices.[27] The number of

[a]*Laboratory for High Performance Ceramics, Empa. Swiss Federal Laboratories for Materials Science and Technology, Überlandstrasse 129, CH-8600 Dübendorf, Switzerland. E-mail: amy.knorpp@empa.ch; michael.stuer@empa.ch*

[b]*Department of Ceramics and Refractories, Faculty of Materials Science and Ceramics, AGH University of Science and Technology, al. Mickiewicza, 30-059 Krakow, Poland*

[c]*Center for X-ray Analytics, Swiss Federal Laboratories for Materials Science and Technology, Empa. Überlandstrasse 129, CH-8600 Dübendorf, Switzerland*

[d]*Energy and Environment Division, Paul Scherrer Insitut, Forschungsstrasse 111, 5232 Villigen PSI, Switzerland*

† Electronic supplementary information (ESI) available. See https://doi.org/10.1039/d2ra05435c

‡ Authors contributed equally.

cations needed to be incorporated for high-entropy classification varies depending on the structure and the cation's sub lattice positions. With this metric, for a spinel structure, the high-entropy distinction only starts with 7 cation or more – thus, were an LDH to be used as a precursor for a high-entropy spinel structure, it would require at least 7 cations. In order to be considered a high-entropy material directly, an LDH would need at least 8 cations.

Currently there have only been a few attempts to synthesize HE-LDHs.[28–30] However, the focus was on only 5 or 6 cations in the LDH structure[28,29] or on identifying the maximum number of cations incorporated.[30] Though these studies are limited, they show that LDHs with a large number of cations can act as electrocatalysts themselves[29] and also confirm that HE-LDHs can be used precursors to high-entropy oxides.[30]

Since this field of high-entropy layered double hydroxides is only just emerging and a promising one, strategies to synthesize them with relevant ranges of cation configurations are now needed. Therefore, this work focuses on the synthesis of multi-cationic layered double hydroxides with 7 or 8 cations by the hydrothermal method. This synthesis study is especially timely as this field of high-entropy materials is expanded to layered double hydroxides.

## 2. Experimental

### 2.1 Synthesis procedure

The synthesis procedure was adapted for multiple cations from a hydrothermal synthesis method originally for two cations (magnesium and aluminum).[26] The cations considered were Mg, Zn, Cu, Ni, Co (as divalent M(II) cations) and Al, Fe, Cr (as trivalent M(III) cations). The molar ratio of M(II) to M(III) cations was kept at 2. In all synthesis batches, a total of 0.005 moles of M(II) cations and a total of 0.0025 moles of M(III) cations were used. This means the molar contribution of each individual metal cation was scaled according to the number of cations of the same valence used in each synthesis formulation.

For each formulation, metal nitrates (weighed according to Table 1) and 2.25 grams of urea were dissolved into 31.25 ml of distilled water. The solution was stirred by magnetic stirrer for 30 minutes. Afterwards, the solutions were poured into stainless steel autoclaves with PTFE-lined vessels with a capacity of 50 ml. The autoclaves containing the solutions were placed in oven under static conditions at 150 °C and 2 h for all syntheses unless otherwise noted. Crystallization times ranging from 1–4 h and temperatures ranging from 120–180 °C were also used for a selected number of syntheses with 8 cations, to study these parameters' effect on the resulting crystalline phase. After the completion of the crystallization time, the autoclaves were cooled to room temperature. The solid fraction was collected by centrifuge and washed three times with deionized water. The obtained powder was left to dry in air in an oven at 120 °C for 16 hours.

### 2.2 Materials and reagents

Eight different nitrates (Sigma-Aldrich and Fluka, all at least 97% purity) were used as raw materials, without additional

Table 1 Compositions of prepared solutions for hydrothermal synthesis

| Composition of prepared solutions (grams) | | | | | | | | | | | | |
|---|---|---|---|---|---|---|---|---|---|---|---|---|
| | M(II) cations | | | | | | M(III) cations | | | | | |
| | $Mg(NO_3)_2\cdot 6H_2O$ | $Zn(NO_3)_2\cdot 6H_2O$ | $Cu(NO_3)_2\cdot 3H_2O$ | $Ni(NO_3)_2\cdot 6H_2O$ | $Co(NO_3)_2\cdot 6H_2O$ | | $Al(NO_3)_2\cdot 9H_2O$ | $Fe(NO_3)_2\cdot 9H_2O$ | $Cr(NO_3)_2\cdot 9H_2O$ | Urea | Water | # of cations |
| 8 Cation | 0.26 | 0.30 | 0.24 | 0.29 | 0.29 | | 0.31 | 0.34 | 0.22 | 2.25 | 31.25 | 8-Cation formulation |
| 7cat – A | — | 0.37 | 0.30 | 0.36 | 0.36 | | 0.31 | 0.34 | 0.33 | 2.25 | 31.25 | 7-Cation formulation |
| 7cat – B | 0.32 | — | 0.30 | 0.36 | 0.36 | | 0.31 | 0.34 | 0.33 | 2.25 | 31.25 | 7-Cation formulation |
| 7cat – C | 0.32 | 0.37 | — | 0.36 | 0.36 | | 0.31 | 0.34 | 0.33 | 2.25 | 31.25 | 7-Cation formulation |
| 7cat – D | 0.32 | 0.37 | 0.30 | — | 0.36 | | 0.31 | 0.34 | 0.33 | 2.25 | 31.25 | 7-Cation formulation |
| 7cat – E | 0.32 | 0.37 | 0.30 | 0.36 | — | | 0.31 | 0.34 | 0.33 | 2.25 | 31.25 | 7-Cation formulation |
| 7cat – F | 0.26 | 0.30 | 0.24 | 0.29 | 0.29 | | — | 0.51 | 0.50 | 2.25 | 31.25 | 7-Cation formulation |
| 7cat – G | 0.26 | 0.30 | 0.24 | 0.29 | 0.29 | | 0.47 | — | 0.50 | 2.25 | 31.25 | 7-Cation formulation |
| 7cat – H | 0.26 | 0.30 | 0.24 | 0.29 | 0.29 | | 0.47 | 0.51 | — | 2.25 | 31.25 | 7-Cation formulation |

purification. The starting materials were the following: magnesium nitrate hexahydrate ($Mg(NO_3)_2 \cdot 6H_2O$, Sigma-Aldrich, >98% purity), zinc nitrate hexahydrate ($Zn(NO_3)_2 \cdot 6H_2O$, Sigma-Aldrich, >98% purity), copper nitrate trihydrate ($Cu(NO_3)_2 \cdot 3H_2O$, Fluka, >98% purity), nickel nitrate hexahydrate ($Ni(NO_3)_2 \cdot 6H_2O$, Fluka, >97% purity), cobalt nitrate hexahydrate ($Co(NO_3)_2 \cdot 6H_2O$, Sigma-Aldrich, >98% purity), aluminium nitrate nonahydrate ($Al(NO_3)_3 \cdot 9H_2O$, Sigma-Aldrich, >98% purity), iron nitrate nonahydrate ($Fe(NO_3)_3 \cdot 9H_2O$, Sigma-Aldrich, >98% purity), chromium nitrate nonahydrate ($Cr(NO_3)_3 \cdot 9H_2O$, Sigma-Aldrich, >99% purity) and urea ($NH_2CONH_2$, Sigma-Aldrich, >98% purity).

# 3. Results and discussion

## 3.1 Solution with 8 cations: synthesis condition variation and resulting crystalline phases

The crystallization time and temperature of 2 h at 150 °C specified in Section 2.2 were arrived at through a synthesis optimization procedure, where crystallization times of 1–4 h and crystallization temperatures of 120, 150, 180 °C were tested with the 8-cation formulation listed in Table 1, to monitor the influence of these conditions on the resulting crystal structure. In order to monitor the formation of layered double hydroxides as well as secondary crystalline phases, an X-ray powder diffraction was performed on all synthesized samples. Experimental and equipment details can be found in the ESI.† Fig. 1 (left) shows the influence of crystallization temperature on the formation of LDHs when 8 cations are present in the starting solution. All patterns exhibit the (003), (006), (009), (012), (015) (018), (110), and (113) characteristic reflections of a layered double hydroxide phase;[31,32] however, at a crystallization temperature of 180 °C and crystallization time of 2 hours, a secondary carbonate phase starts to form. Conversely at lower crystallization temperatures, reflections for the LDH structure appear broad with low intensity, likely due to low crystallinity. In Fig. 1 (right), the crystallization time and temperature were both varied in order to find synthesis conditions which produced pure LDH for each crystallization temperature.

Overall, LDHs from 8-cation solutions can be synthesized within a considerable range of crystallization temperatures and times common in hydrothermal synthesis. Pure and crystalline LDH could be observed for temperature range of 150–180 °C, though the time needed was longer at 150 °C, needing 2 h, compared to 1 h at 180 °C.

## 3.2 Solutions with 7 cations: synthesis and resulting crystalline phases

The crystallization temperature of 150 °C and time of 2 hours were selected to perform the syntheses of the series of 7-cation solutions. The '—' in Table 1 represent which cation from the 8 cations was not included in each 7-cation solution, and Fig. 2 shows the X-ray powder diffraction patterns for all 7-cation syntheses. All of these led to LDH as the major crystalline phase.

## 3.3 Characterization of 8-cation LDH and 7-cation LDH

**3.3.1 Morphology.** Platy morphology is often observed for the hydrothermal synthesis of hydrotalcite-like structure with only two cation (Al and Mg),[32] and it appears that even at 7 or more cations, this platy morphology also develops. Fig. 3 shows the morphology of the 8-cation LDH sample as observed by scanning electron microscope. The plates appear to be heavily agglomerated. To estimate the crystallite size, the Scherrer equation was used for [003] reflection, and the crystallites were estimated to be about 14 nm.

Similar morphology of agglomerated platelets were observed for all the 7-cation formulations. It appears these LDHs heavily favor the formation of platelets despite the varying number of cations, chemistries, or synthesis conditions.

**3.3.2 Chemical analysis.** To further understand the chemical nature of this multi-cationic LDH structure, SEM/EDS and X-ray absorption were conducted on the 8-cation LDH.

One criterion for high entropy materials is that elements are homogeneously distributed throughout the structure. To confirm homogeneous distribution, EDS elemental mapping

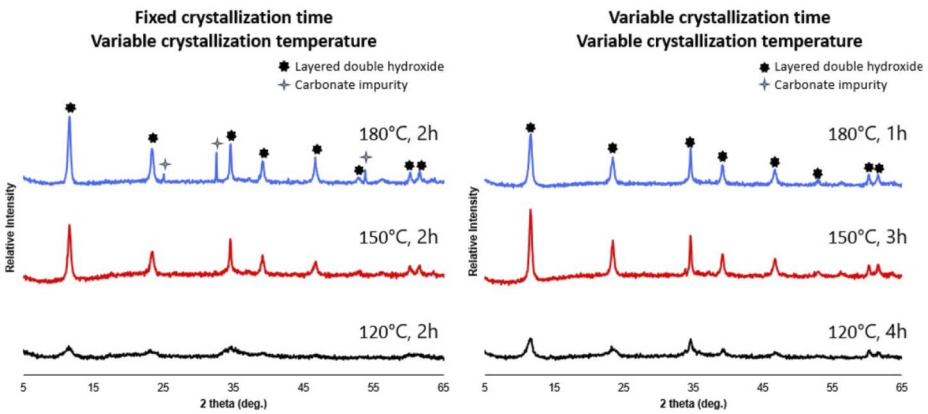


Fig. 1 (Left) Resulting X-ray diffraction patterns for syntheses conducted with a fixed crystallization time of 2 hours and variable crystallization temperatures for a solution of 8 cations. (Right) Resulting X-ray diffraction patterns where both the temperature and time were varied in order to achieve pure LDH.

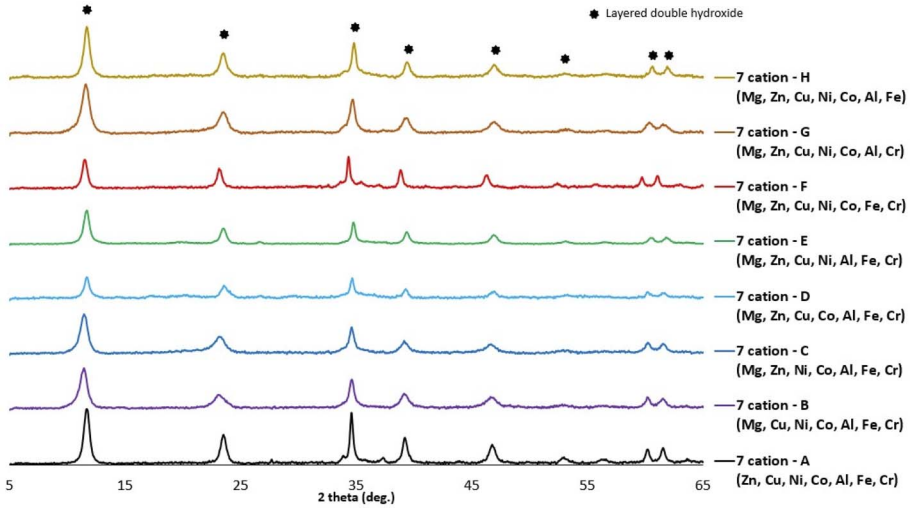


Fig. 2 X-ray diffraction patterns of all synthesized LHDs with 7-cation in the starting solution. Hydrothermal synthesis was conducted with crystallization time of 2 h and crystallization temperature of 150 °C.

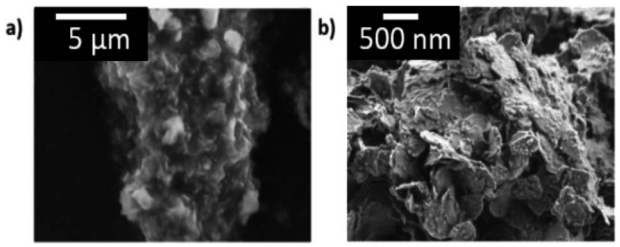


Fig. 3 Secondary micrograph of as-synthesized 8-cation LDH with image (a) at low magnification and (b) at high magnification. Large agglomerates of platelets were observed.

was conducted. Fig. 4 shows SEM EDS maps of the 8-cation LDH. No tendency of segregation of cations was observed for the 8-cation LDH.

Atomic concentrations for each element were also estimated by EDS. Ideally elements of similar oxidation states should be equimolar, in order to increase the configurational entropy. Table 2 shows atomic concentrations of elements for the 8-cation LDH and all 7-cation LDHs. Measurements were taken on five different particles and averaged. Across all formulations, zinc and copper were found to exhibit the poorest incorporation, while aluminum and magnesium have slightly higher incorporation than expected. Of the M(II) cations, nickel and cobalt mostly exhibit the expected amounts and are equimolar to each other; similarly, for the M(III) cations, iron and chromium are as expected in concentration and are equimolar to each other. Of all the samples, 7cat-H (Mg, Cu, Zn, Ni, Co, Al, Fe) is the closest of the samples to achieving an equimolar distribution, but even though the copper amount is higher than in the other 7-cation formulations, it still below the amount needed for equimolarity. The final M(II) and M(III) ratio is slightly lower than the starting M(II) and M(III) ratio (1.3–1.6 rather than 2). This discrepancy is likely due to the poor incorporation of copper and zinc. The remaining liquid from the synthesis was a brown/bluish color and likely contained cations that were not fully incorporated in the LDH. There appears to be preference for incorporating certain cations over others.

The transition metals substituted into the LDHs in this study can exist in many different oxidation states. To confirm the oxidation state of the transition metals (Fe, Cr, Co, Ni, Zn and Cu), and evaluate the effect of the removal of specific cations from the structure on oxidation states, X-ray absorption spectroscopy (XAS) was performed on the 8-cation LDH and one 7-cation LDH (7cat-H with Mg, Zn, Cu, Co, Ni, Al, Fe). The edge position in the XANES region of the XAS spectra can indicate the oxidation state. Since the oxidation state is known for the nitrate precursors, these were used as a reference for the oxidation state in the LDHs. Analysis of XAS data was conducted on the demeter software.[33] The edge positions for the LDH samples were not significantly shifted from the nitrate references as shown in Fig. S8.† Therefore, there appears to be no oxidation–reduction chemistry occurring during the synthesis to accommodate the multitude of cations into the structure.

Fig. 5 shows the EXAFS spectra $k^3\chi(k)$ and the real space $\chi(R)$ for Cu, Zn, Ni, Co, Cr, and Fe. For all probed cations, the $\chi(R)$ spectrum is consistent with a layered double hydroxide system. The first peak (1–2 Å) corresponds to the scattering between the cation absorber and the nearest oxygen neighbour, and the second peak (2.5–3.5 Å) corresponds to the scattering between the cation absorber and the second shell that is populated by other cations. The EXAFS spectra suggest that the nickel, cobalt, and zinc have similar scattering environments. The similar local geometry of nickel, cobalt, and zinc in the LDH structure is further corroborated by fitting of the first shell where obtained coordination numbers are 6.1 ± 0.7, 6.0 ± 0.8, and 6.0 ± 0.7 respectively, and the distances between each probed cation and nearest oxygen was 2.05 Å ± 0.01, 2.06 Å ± 0.01, and 2.03 Å ± 0.02, respectively. Of the M(II) cations, copper is the outlier with a distinctly different EXAFS

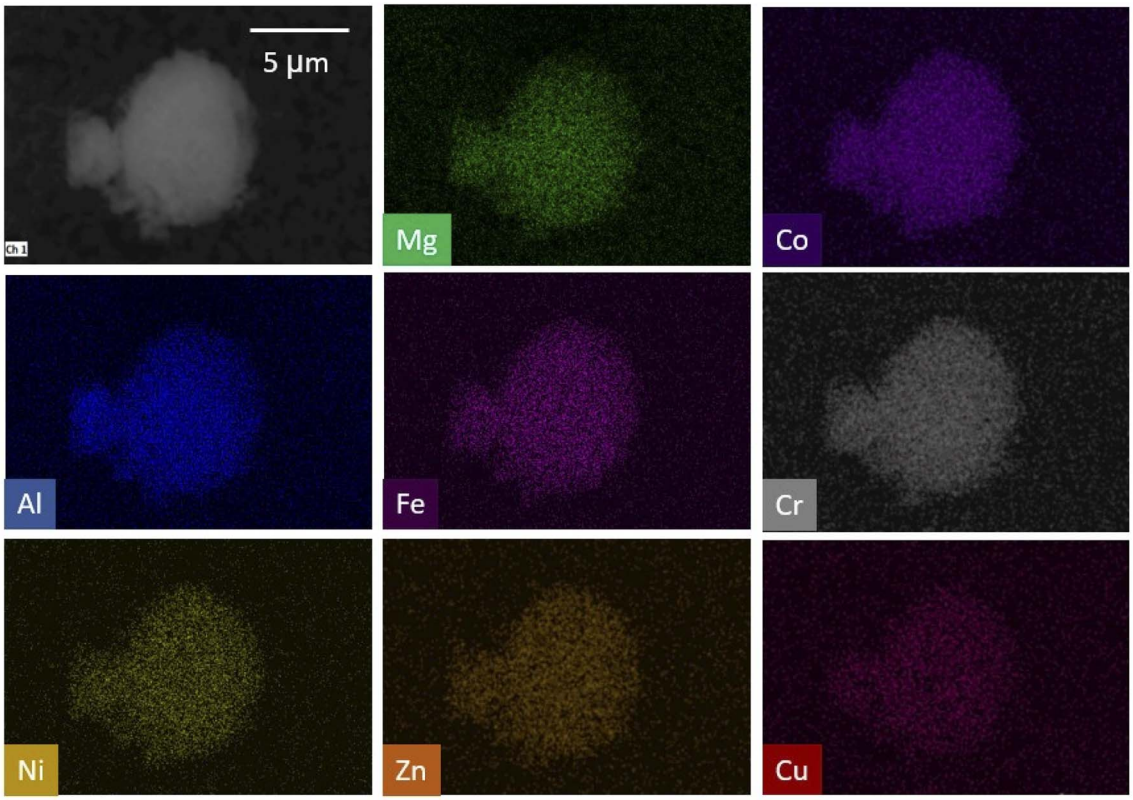


Fig. 4 EDS spectra and mapping of 8-cation LDH. Cations appear to be well-dispersed throughout the structure.

spectrum and initial fittings showing a lower than expected coordination number (3.9 ± 0.4), and indicate possible Jahn–Teller distortion.[34–36]

The EXAFS spectra for chromium and iron show that these M(III) cations have a local geometry different from the M(II) cations. The first shell scattering is shorter for M(III) than for M(II) cations, with the nearest oxygen neighbour for iron and chromium being 1.98 Å ± 0.02 and 1.99 Å ± 0.02, respectively. This different in distances between M(II) and M(III) cations has also been observed from LHDs with two or three cations incorporated as well.[37] However, the coordination of the iron and chromium is lower than expected with 5.5 ± 0.9 and 5.0 ± 0.9, respectively.

The 7-cation sample (7cat-H) shows generally similar coordination numbers and distances for first shell scattering events as the 8-cation LDH. High resolution X-ray powder diffraction was also conducted on both the 8-cation and 7cat-H samples. The calculated lattice parameters are summarized in Table 3 where the unit cell parameter $c$ ($=3d_{003}$) corresponds to three times the interlayer distance and $a$ ($=2d_{110}$) is the average distance between the two cations. Generally little geometry and structural differences were observed between the 7-cation (7cat-

Table 2 EDS analysis of atomic concentration of elements in synthesized samples. The atomic concentration for each element was averaged from 5 different particles

| Atomic concentration (%) by EDS analysis | | | | | | | | | |
|---|---|---|---|---|---|---|---|---|---|
| Oxidation state (confirmed by XAS) | M(II) cations | | | | | M(III) cations | | | M(II)/M(III) |
| | Mg | Zn | Cu | Ni | Co | Al | Fe | Cr | |
| 8 Cation | 16.9 ± 1.2 | 9.0 ± 0.3 | 4.6 ± 0.2 | 14.3 ± 0.8 | 14.4 ± 1.3 | 16.1 ± 0.8 | 12.1 ± 0.4 | 12.3 ± 0.5 | 1.5 |
| 7cat – A | — | 10.9 ± 0.3 | 4.4 ± 0.2 | 20.2 ± 0.3 | 20.6 ± 0.4 | 16.0 ± 0.8 | 13.6 ± 0.1 | 14.3 ± 0.1 | 1.3 |
| 7cat – B | 17.8 ± 1.0 | — | 7.6 ± 0.3 | 17.7 ± 0.6 | 18.6 ± 0.4 | 14.3 ± 0.5 | 12.0 ± 0.1 | 12.0 ± 0.2 | 1.6 |
| 7cat – C | 19.9 ± 1.4 | 8.8 ± 0.6 | — | 15.6 ± 0.5 | 17.2 ± 0.4 | 15.1 ± 0.4 | 11.6 ± 0.2 | 11.7 ± 0.2 | 1.6 |
| 7cat – D | 21.4 ± 2.4 | 11.7 ± 1.2 | 8.1 ± 1.1 | — | 17.5 ± 0.6 | 16.8 ± 1.6 | 12.0 ± 0.7 | 12.5 ± 0.7 | 1.4 |
| 7cat – E | 22.8 ± 1.5 | 11.7 ± 0.5 | 4.0 ± 0.2 | 19.1 ± 0.8 | — | 15.4 ± 0.7 | 13.3 ± 0.6 | 13.6 ± 0.6 | 1.4 |
| 7cat – F | 15.2 ± 1.0 | 8.0 ± 0.3 | 4.1 ± 0.2 | 15.1 ± 0.4 | 17.0 ± 0.2 | — | 20.3 ± 0.1 | 20.3 ± 0.3 | 1.5 |
| 7cat – G | 17.1 ± 2.0 | 9.6 ± 0.6 | 4.7 ± 0.4 | 13.3 ± 0.7 | 14.0 ± 0.9 | 23.3 ± 1.5 | — | 17.9 ± 0.9 | 1.5 |
| 7cat – H | 12.7 ± 0.5 | 11.5 ± 0.6 | 8.2 ± 0.5 | 13.1 ± 0.5 | 13.8 ± 0.6 | 21.0 ± 0.7 | 19.6 ± 2.9 | — | 1.5 |

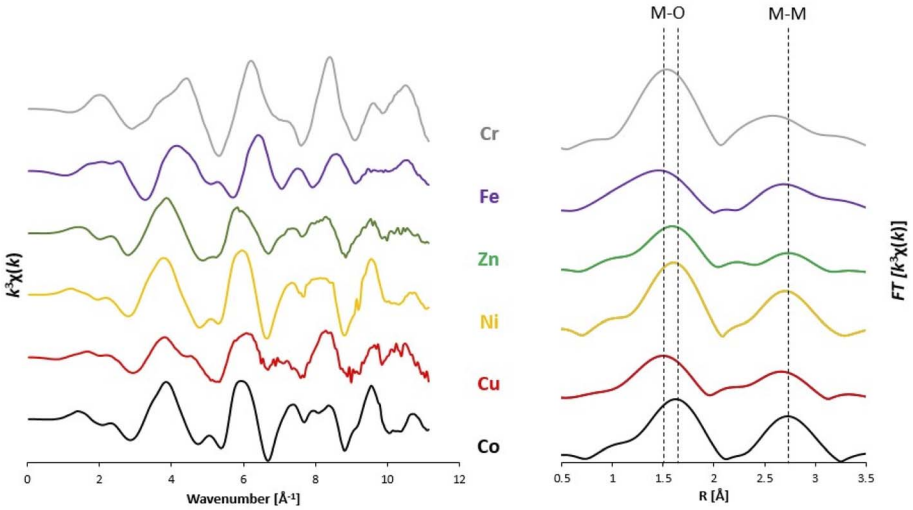


Fig. 5 (Left) EXAFS spectra of Cr, Fe, Zn, Ni, Cu, and Co for 8-cation LDH. (Right) The Fourier transform of the $k^3\chi(k)$ taken using the range of $k$ = 2.5–10 Å$^{-1}$. Scattering distances are uncorrected for phase-shift.

H) and 8-cation systems by XRD and XAS. The multitude of incorporated cations could dampen any changes in the local structure when specific cations are omitted or included.

### 3.4 Magnetic properties

In order to investigate the magnetic properties of the 8-cation sample, we performed DC magnetization measurements by collecting temperature-dependent zero field cooling (ZFC) and field cooling (FC) magnetization $M(T)$ data under various external magnetic fields (Fig. 6a) and by measuring magnetization $M(H)$ loops at different temperatures (Fig. 6b). From Fig. 6a and b, it can be observed that the 8-cation LDH shows a rather complex magnetic response.

For $M(T)$ measured between 5 and 90 K, a separation between ZFC and FC can be observed below $T \approx 45$ K when exposed to magnetic fields $\mu_0 H \leq 0.1$ T, indicative of a history-dependent behavior. In high magnetic fields (*i.e.*, $\mu_0 H \approx 1$ T), however, the $M(T)$ curve appears to fully overlap in the measured temperature range and within the resolution limit of the measurement. In Fig. 6b, we show corresponding magnetization $M(H)$ loops taken at 5, 15, 30, 60, and 90 K, respectively. Above ≈30 K, the $M(H)$ curves display almost a linear magnetic field dependence without any hysteresis signs, suggesting a paramagnetic behavior. A hysteretic behavior appears at temperatures ≤30 K, with coercivity ranging from ≈0.019 T at 5 K to ≈0.006 T at 30 K (inset of Fig. 6b), respectively, reminiscent of a ferromagnetic-like behavior.

Because of the observed paramagnetic to ferromagnetic-like behavior transition, additional time-dependent magnetization experiments were performed on the same 8-cation LDH. These included AC magnetic susceptibility measurements with AC frequencies between 1 and 300 Hz in absence of a static external magnetic field, as well as aging and memory experiments for the DC magnetization, as shown in Fig. 6c. A frequency-dependent behavior is observed in the temperature-dependent real part of the AC susceptibility $\chi'(T)$ at temperatures ranging from ≈10 to ≈60 K (Fig. 6c). Moreover, a plateau can be observed, the shoulder of which shifts with increasing frequency from ≈33 to ≈40 K, while its amplitude decrease gradually, which may suggest a possible spin-glass freezing behavior.

The frequency dependence of the $\chi'(T)$ plateaus in the AC magnetization measurements were further analyzed and fitted to a critical dynamical scaling model[38] as well as the Vogel–Fulcher model.[39] The fits can be found in the inset of Fig. 6c, and the fitting parameters can be found in the ESI.† The fitting results allowed to further corroborate the suggested spin-glass of the 8-cation LDH with a freezing temperature $T_s$ of ≈30 K.

Memory and aging effects are additional experimental signatures of a spin-glass behavior in magnetic materials.[40] Therefore, FC memory and aging effects were studied by intermittent-stop cooling (ISC) and continuous warming (CW) as shown in Fig. 6d. In the spin-glass state, a magnetization shift can be observed when the cooling is resumed (Fig. 6d). In the CW process, the sample is continuously heated up from 5 to

Table 3 Structural parameters of 8-cation LDH and 7cat-H

| | Lattice parameters | | | |
|---|---|---|---|---|
| | $d$(003) Å | $d$(110) Å | $a$ (Å) | $c$ (Å) |
| 8-Cation (Mg, Zn, Cu, Ni, Co, Al, Fe, Cr) | 7.66 | 1.54 | 3.07 | 22.97 |
| 7cat-H (Mg, Zn, Cu, Ni, Co, Al, Fe) | 7.68 | 1.53 | 3.06 | 23.05 |

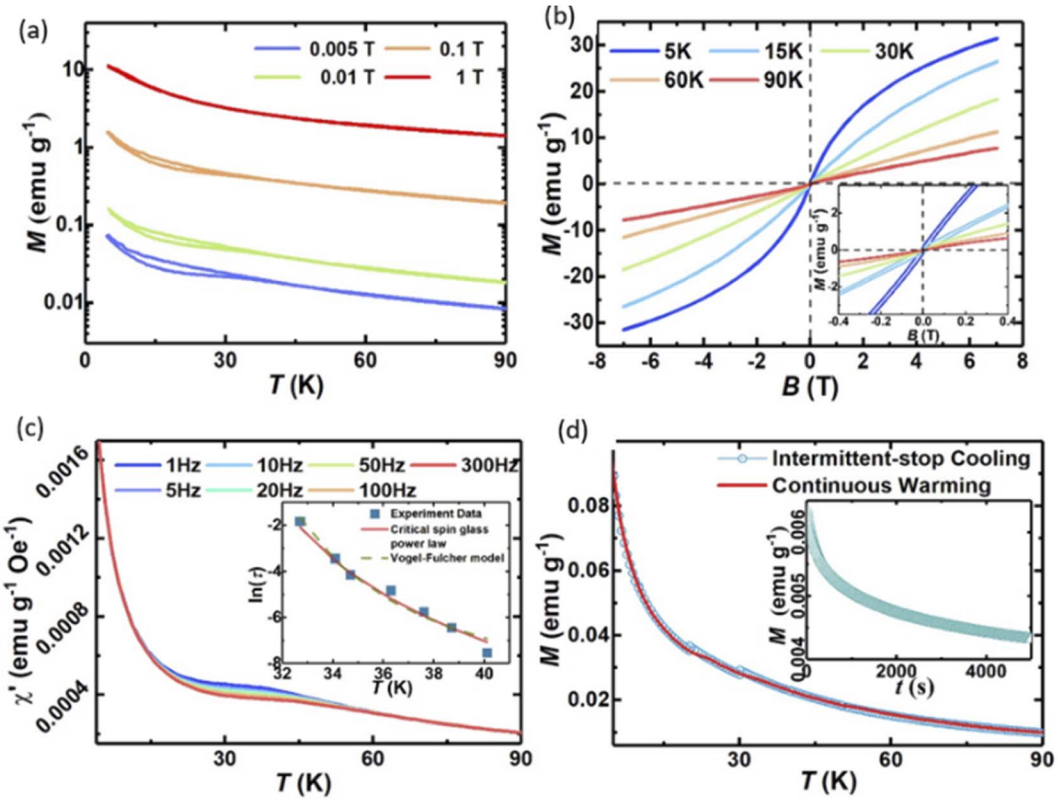


Fig. 6 (a) Temperature-dependent ZFC (lower lines) and FC (upper lines) magnetization $M(T)$ measurements on 8-cation LDH in external magnetic fields $B$ ($\mu_0 H$) = 0.005, 0.01, 0.1, and 1 T, respectively; (b) isothermal magnetization $M(H)$ loops with mag magnetic fields ranging from −7 to 7 T in temperatures between 5 and 90 K, inset of (b) an expanded scale to show the hysteretic behavior in low magnetic fields. (c) Real part ($\chi'$) of the AC susceptibility as a function of temperature and frequency from 1 Hz to 300 Hz, inset of (c) measurement period ($\tau = 1/2\pi f$ where $f$ is the frequency of applied magnetic field) *vs.* peak temperatures of the real part of the AC magnetic susceptibility $\chi'$; (d) aging and memory measurements according to intermittent-stop cooling (ISC) and continuous warming-up (CW) processes, respectively, in an external field of 5 mT, with a waiting time in the ISC process of 5000 s, inset of (b) the time dependence of the magnetic moment (triangle) at 25 K after switching off the magnetic field.

90 K under a constant magnetic field (5 mT) following an ISC run. The CW magnetization $M(T)$ exhibits kink-like features at the previous intermittent-stopping temperatures (below the spin-glass freezing temperature) suggesting a memory effect characteristic for many spin-glasses.[40–42] In spin-glass states, spin dynamics are known to slow down whilst approaching the freezing temperature $T_s$, impeding the magnetization recovery and provoking measurable magnetization steps in ISC curves.[43]

Following this discussion, it is worth noting that superconductivity has been previously observed in hydroxide materials, albeit only under high mechanical pressure.[44] Since mechanical and chemical pressures similarly allow changing the Fermi surface of the sample, it may be suggested that a high chemical pressure may be reached *via* compositional changes and/or high-entropy structures which may allow reaching superconductivity. Note also that in some superconductive systems, spin-glass states and superconductor states are not independent, meaning that *via* elemental and/or structural tuning a shift from a spin-glass to a superconductor state may be achievable. More research is therefore needed in order to corroborate whether HE-LDH may be able to become superconductive.

## 4. HE-LDHs in the context of high-entropy materials

Recently different nomenclature has emerged to categorize high-entropy materials, specifically in reference to oxides, where materials have been labeled as entropy-stabilized oxides (ESO) and/or high-entropy oxides (HEO). Although these terms had often been used interchangeably, there has been recent discussion of clarifying these definitions.[27,45–47] Since multi-cationic LDHs are only just emerging, it is pertinent to ask how they fit generally into the high-entropy materials discussion.

Entropy-stabilized materials possess configurational entropy that drives the stabilization of a single phase and often have equivalent concentration of all cations. The most elegant examples of these materials are entropy-stabilized rock salt[4] and a fluorite oxide,[45] where reversibility of multiple phases to a single phase can be observed during different annealing temperatures. In the case of HE-LDHs, it would be difficult to confirm entropy stabilization using this technique, as LDHs are not stable at elevated temperatures due to its very nature. No

thermal stability advantages were observed in the 8-cation LDH in comparison with hydrotalcite (2 cations incorporated) during thermogravimetric analysis (ESI, Fig. S7†).

Multicationic LDHs will likely not fall into the entropy-stabilized category of high-entropy materials from the high temperature criterion, which however may not rightfully be applicable here. The field of HE-LDHs, however, should in any case fall in the broader definition of high-entropy materials, where the number of different cations and their concentrations (equivalent or non-equivalent to each other) contribute to the increased configurational entropy leading to interesting properties from cocktail effects and/or lattice distortions. Additionally, the role of high entropy in precursors to high-entropy oxides is yet to be fully explored, and may prove to have advantages in reducing calcination and sintering temperatures as well as expand the range of elements incorporated into an oxide structure.

## 5. Conclusions

In this work, we present a hydrothermal synthesis method for obtaining high-entropy layered double hydroxides, which represent an emerging branch of high-entropy materials.

A total of eight formulations using 7 or 8 cations (Mg, Cu, Zn, Co, Ni, Al, Fe, Cr) were successfully synthesized, with the incorporated elements showing a homogeneous distribution in the structure with oxidation state inherited from the metal salts. The 7-cation LDHs incorporated a wide range of different chemistries, highlighting the tailorability of this material class and opening the door for synthesis of further materials. Considering the number of possible combinations as well as the number of cations and their nature, many types of high-entropy hydroxides can be synthesized with properties still waiting to be investigated. The present study provides an important foundational synthesis of these materials, a required first step on the way to future investigations and applications.

## Conflicts of interest

There are no conflicts to declare.

## References

1 B. Cantor, I. T. H. Chang, P. Knight and A. J. B. Vincent, Microstructural development in equiatomic multicomponent alloys, *Mater. Sci. Eng. A*, 2004, **375–377**, 213–218, DOI: **10.1016/j.msea.2003.10.257**.

2 J. W. Yeh, S. K. Chen, S. J. Lin, J. Y. Gan, T. S. Chin, T. T. Shun, C. H. Tsau and S. Y. Chang, Nanostructured high-entropy alloys with multiple principal elements: Novel alloy design concepts and outcomes, *Adv. Eng. Mater.*, 2004, **6**, 299–303, DOI: **10.1002/adem.200300567**.

3 A. Amiri and R. Shahbazian-Yassar, Recent progress of high-entropy materials for energy storage and conversion, *J. Mater. Chem. A*, 2021, 782–823, DOI: **10.1039/d0ta09578h**.

4 C. M. Rost, E. Sachet, T. Borman, A. Moballegh, E. C. Dickey, D. Hou, J. L. Jones, S. Curtarolo and J. P. Maria, Entropy-stabilized oxides, *Nat. Commun.*, 2015, **6**, 8485, DOI: **10.1038/ncomms9485**.

5 J. Gild, Y. Zhang, T. Harrington, S. Jiang, T. Hu, M. C. Quinn, W. M. Mellor, N. Zhou, K. Vecchio and J. Luo, High-Entropy Metal Diborides: A New Class of High-Entropy Materials and a New Type of Ultrahigh Temperature Ceramics, *Sci. Rep.*, 2016, **6**, 2–11, DOI: **10.1038/srep37946**.

6 E. Castle, T. Csanádi, S. Grasso, J. Dusza and M. Reece, Processing and Properties of High-Entropy Ultra-High Temperature Carbides, *Sci. Rep.*, 2018, **8**, 1–12, DOI: **10.1038/s41598-018-26827-1**.

7 C. H. Lai, S. J. Lin, J. W. Yeh and S. Y. Chang, Preparation and characterization of AlCrTaTiZr multi-element nitride coatings, *Surf. Coat. Technol.*, 2006, **201**, 3275–3280, DOI: **10.1016/j.surfcoat.2006.06.048**.

8 C. F. Wu, D. E. S. Arifin, C. A. Wang and J. Ruan, Coalescence and split of high-entropy polymer lamellar cocrystals, *Polymer (Guildf).*, 2018, **138**, 188–202, DOI: **10.1016/j.polymer.2018.01.064**.

9 T. Wang, H. Chen, Z. Yang, J. Liang and S. Dai, High-Entropy Perovskite Fluorides: A New Platform for Oxygen Evolution Catalysis, *J. Am. Chem. Soc.*, 2020, **142**, 4550–4554, DOI: **10.1021/jacs.9b12377**.

10 R. Z. Zhang, F. Gucci, H. Zhu, K. Chen and M. J. Reece, Data-Driven Design of Ecofriendly Thermoelectric High-Entropy Sulfides, *Inorg. Chem.*, 2018, **57**, 13027–13033, DOI: **10.1021/acs.inorgchem.8b02379**.

11 Z. Lei, X. Liu, H. Wang, Y. Wu, S. Jiang and Z. Lu, Development of advanced materials via entropy engineering, *Scr. Mater.*, 2019, **165**, 164–169, DOI: **10.1016/j.scriptamat.2019.02.015**.

12 A. Salian and S. Mandal, Entropy stabilized multicomponent oxides with diverse functionality–a review, *Crit. Rev. Solid State Mater. Sci.*, 2021, 1–52, DOI: **10.1080/10408436.2021.1886047**.

13 W. T. Reichle, Synthesis of anionic clay minerals (mixed metal hydroxides, hydrotalcite), *Solid State Ionics*, 1986, **22**, 135–141, DOI: **10.1016/0167-2738(86)90067-6**.

14 F. Cavani, F. Trifirò and A. Vaccari, Hydrotalcite-type anionic clays: Preparation, properties and applications, *Catal. Today*, 1991, **11**, 173–301, DOI: **10.1016/0920-5861(91)80068-K**.

15 Q. Wang and D. Ohare, Recent advances in the synthesis and application of layered double hydroxide (LDH) nanosheets, *Chem. Rev.*, 2012, **112**, 4124–4155, DOI: **10.1021/cr200434v**.

16 G. Fan, F. Li, D. G. Evans and X. Duan, Catalytic applications of layered double hydroxides: Recent advances and perspectives, *Chem. Soc. Rev.*, 2014, **43**, 7040–7066, DOI: **10.1039/c4cs00160e**.

17 Z. P. Xu, J. Zhang, M. O. Adebajo, H. Zhang and C. Zhou, Catalytic applications of layered double hydroxides and derivatives, *Appl. Clay Sci.*, 2011, **53**, 139–150, DOI: **10.1016/j.clay.2011.02.007**.

18 G. Arrabito, A. Bonasera, G. Prestopino, A. Orsini, A. Mattoccia, E. Martinelli, B. Pignataro and P. G. Medaglia, Layered double hydroxides: A toolbox for chemistry and biology, *Crystals*, 2019, **9**, 361, DOI: **10.3390/cryst9070361**.

19 V. Rives, M. del Arco and C. Martín, Intercalation of drugs in layered double hydroxides and their controlled release: A review, *Appl. Clay Sci.*, 2014, **88–89**, 239–269, DOI: **10.1016/j.clay.2013.12.002**.

20 A. M. Cardinale, C. Carbone, S. Consani, M. Fortunato and N. Parodi, Layered double hydroxides for remediation of industrial wastewater from a Galvanic plant, *Crystals*, 2020, **10**, 443, DOI: **10.3390/cryst10060443**.

21 Z. Yang, F. Wang, C. Zhang, G. Zeng, X. Tan, Z. Yu, Y. Zhong, H. Wang and F. Cui, Utilization of LDH-based materials as potential adsorbents and photocatalysts for the decontamination of dyes wastewater: A review, *RSC Adv.*, 2016, **6**, 79415–79436, DOI: **10.1039/c6ra12727d**.

22 L. Feng and X. Duan Applications of layered double hydroxides, in *Structure and Bonding*, ed. Duan X. and Evans D. G., Springer-Verlag, 2006, pp. 193–223.

23 T. Hibino, Y. Yamashita, K. Kosuge and A. Tsunashima, Decarbonation Behavior of Mg-Al-$CO_3$ Hydrotalcite-like Compounds during Heat Treatment, *Clays Clay Miner.*, 1995, **43**, 427–432, DOI: **10.1346/CCMN.1995.0430405**.

24 F. Li, J. Liu, D. G. Evans and X. Duan, Stoichiometric Synthesis of Pure MFe2O4 (M = Mg, Co, and Ni) Spinel Ferrites from Tailored Layered Double Hydroxide (Hydrotalcite-Like) Precursors, *Chem. Mater.*, 2004, **16**, 1597–1602, DOI: **10.1021/cm035248c**.

25 J. G. Li, T. Ikegami, J. H. Lee, T. Mori and Y. Yajima, Synthesis of Mg-Al spinel powder via precipitation using ammonium bicarbonate as the precipitant, *J. Eur. Ceram. Soc.*, 2001, **21**, 139–148, DOI: **10.1016/S0955-2219(00)00188-6**.

26 Z. P. Xu and H. C. Zeng, Control of surface area and porosity of $Co_3O_4$ via intercalation of oxidative or nonoxidative anions in hydrotalcite-like precursors, *Chem. Mater.*, 2000, **12**, 3459–3465, DOI: **10.1021/cm000371e**.

27 O. F. Dippo and K. S. Vecchio, A universal configurational entropy metric for high-entropy materials, *Scr. Mater.*, 2021, **201**, 113974, DOI: **10.1016/j.scriptamat.2021.113974**.

28 A. Miura, S. Ishiyama, D. Kubo, N. C. Rosero-Navarro and K. Tadanaga, Synthesis and ionic conductivity of a high-entropy layered hydroxide, *J. Ceram. Soc. Jpn.*, 2020, **128**, 336–339, DOI: **10.2109/jcersj2.20001**.

29 K. Gu, X. Zhu, D. Wang, N. Zhang, G. Huang, W. Li, P. Long, J. Tian, Y. Zou, Y. Wang, *et al.*, Ultrathin defective high-entropy layered double hydroxides for electrochemical water oxidation, *J. Energy Chem.*, 2021, **60**, 121–126, DOI: **10.1016/j.jechem.2020.12.029**.

30 M. Kim, I. Oh, H. Choi, W. Jang, J. Song, C. S. Kim, J.-W. Yoo and S. Cho, A solution-based route to compositionally complex metal oxide structures using high-entropy layered double hydroxides, *Cell Rep. Phys. Sci.*, **2021**, 100702, DOI: **10.1016/j.xcrp.2021.100702**.

31 M. Jabłońska, L. Chmielarz, A. Węgrzyn, K. Guzik, Z. Piwowarska, S. Witkowski, R. I. Walton, P. W. Dunne and F. Kovanda, Thermal transformations of Cu-Mg (Zn)-Al(Fe) hydrotalcite-like materials into metal oxide systems and their catalytic activity in selective oxidation of ammonia to dinitrogen, *J. Therm. Anal. Calorim.*, 2013, **114**, 731–747, DOI: **10.1007/s10973-012-2935-9**.

32 M. M. Rao, B. R. Reddy, M. Jayalakshmi, V. S. Jaya and B. Sridhar, Hydrothermal synthesis of Mg-Al hydrotalcites by urea hydrolysis, *Mater. Res. Bull.*, 2005, **40**, 347–359, DOI: **10.1016/j.materresbull.2004.10.007**.

33 B. Ravel and M. Newville, ATHENA, ARTEMIS, HEPHAESTUS: Data analysis for X-ray absorption spectroscopy using IFEFFIT, *J. Synchrotron Radiat.*, 2005, **12**, 537–541, DOI: **10.1107/S0909049505012719**.

34 C. M. Rost, Z. Rak, D. W. Brenner and J. P. Maria, Local structure of the $Mg_xNi_xCo_xCu_xZn_xO$ (x = 0.2) entropy-stabilized oxide: An EXAFS study, *J. Am. Ceram. Soc.*, 2017, **100**, 2732–2738, DOI: **10.1111/jace.14756**.

35 F. Leroux, E. M. Moujahid, H. Roussel, A.-M. Flank, V. Briois and J.-P. Besse, Local order of the transition metals for the substitution (Co1 - yCuy)2Al(OH)6Cl·n$H_2O$(0 4 y 4 1 ) in a copper-aluminum-layered double hydroxide-like phase, *Clays Clay Miner.*, 2002, **50**, 254–264.

36 M. Köckerling, G. Geismar, G. Henkel and H. F. Nolting, X-Ray absorption spectroscopic studies on copper-containing hydrotalcite, *J. Chem. Soc., Faraday Trans.*, 1997, **93**, 481–484, DOI: **10.1039/a605289d**.

37 H. Roussel, V. Briois, E. Elkaim, A. De Roy and J. P. Besse, Cationic order and structure of [Zn-Cr-CI] and [Cu-Cr-Cl] layered double hydroxides: A XRD and EXAFS study, *J. Phys. Chem. B*, 2000, **104**, 5915–5923, DOI: **10.1021/jp0000735**.

38 P. C. Hohenberg and B. I. Halperin, Theory of dynamic critical phenomena, *Rev. Mod. Phys.*, 1977, **49**, 435–479, DOI: **10.1103/RevModPhys.49.435**.

39 H. Vogel, The law of the relation between the viscosity of liquids and the temperature, *Phys. Z.*, 1921, **22**, 645.

40 K. Jonason, P. Nordblad, E. Vincent, J. Hammann and J. P. Bouchaud, Memory interference effects in spin glasses, *Eur. Phys. J. B*, 2000, **13**, 99–105, DOI: **10.1007/s100510050014**.

41 J. R. Dahn, J. E. Greedan, C. V. Stager, G. Liu, I. Davidson and U. Von Sacken, Spin Glass Behaviour in the Frustrated Antiferromagnetic $LiNiO_2$, *J. Solid State Chem.*, 1993, **102**, 542–552.

42 A. Chatterjee, S. Majumdar, S. Chatterjee, A. C. Dippel, O. Gutowski, M. V. Zimmermann and S. Giri, Magnetoelastic coupling at spin-glass-like transition in $Sr_3NiSb_2O_9$, *J. Alloys Compd.*, 2019, **778**, 30–36, DOI: **10.1016/j.jallcom.2018.11.074**.

43 L. W. Bernardi, H. Yoshino, K. Hukushima, H. Takayama, A. Tobo and A. Ito, Aging of the zero-field-cooled magnetization in Ising spin glasses: experiment and numerical simulation, *Phys. Rev. Lett.*, 2001, **86**, 720–723, DOI: **10.1103/PhysRevLett.86.720**.

44 P. Tsuppayakorn-aek, N. Phaisangittisakul, R. Ahuja and T. Bovornratanaraks, High-temperature superconductor of sodalite-like clathrate hafnium hexahydride, *Sci. Rep.*, 2021, **11**, 1–7, DOI: **10.1038/s41598-021-95112-5**.

45 K. Chen, X. Pei, L. Tang, H. Cheng, Z. Li, C. Li, X. Zhang and L. An, A five-component entropy-stabilized fluorite oxide, *J.*

*Eur. Ceram. Soc.*, 2018, **38**, 4161–4164, DOI: **10.1016/j.jeurceramsoc.2018.04.063**.

46 S. H. Albedwawi, A. AlJaberi, G. N. Haidemenopoulos and K. Polychronopoulou, High Entropy Oxides-Exploring a Paradigm of Promising Catalysts: A Review, *Mater. Des.*, 2021, **202**, 109534, DOI: **10.1016/j.matdes.2021.109534**.

47 S. J. McCormack and A. Navrotsky, Thermodynamics of high entropy oxides, *Acta Mater.*, 2021, **202**, 1–21, DOI: **10.1016/j.actamat.2020.10.043**.